Electronic Supplementary Information

for the article

Luminescent Organic Dyes Containing Phenanthro[9,10-D]Imidazole Core and $[Ir(N^C)(N^N)]^+$ Complexes Based on the Cyclometalating and Diimine Ligands of This Type

Anastasia I. Solomatina[1], Kirill M. Kuznetsov[1], Vladislav V. Gurzhiy[2], Vladimir V. Pavlovskiy[1], Vitaly V. Porsev[1], Robert A. Evarestov[1] and Sergey P. Tunik[1]*.

[1]St. Petersburg State University, Institute of Chemistry, Universitetskii pr. 26, 198504 St. Petersburg, Russia.

[2]St. Petersburg State University, Institute of Earth Sciences, University emb. 7/9, 199034 Saint Petersburg, Russia

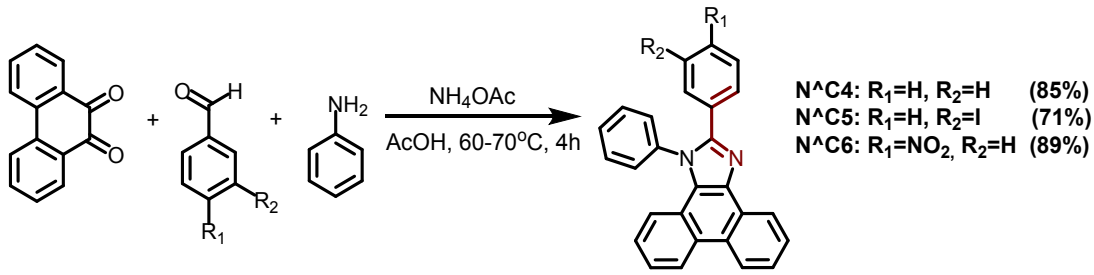

Scheme S1. Synthesis of N^C4- N^C6 ligands.

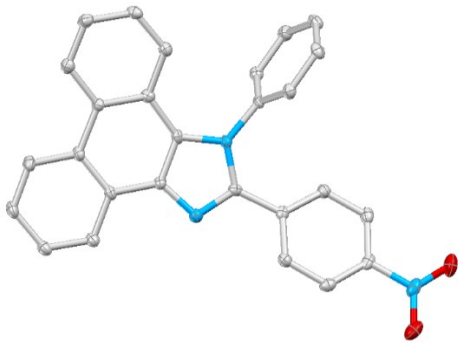

Figure S1. Perspective views of N^C6 showing thermal ellipsoids at the 40% probability level. Hydrogen atoms are omitted for clarity.

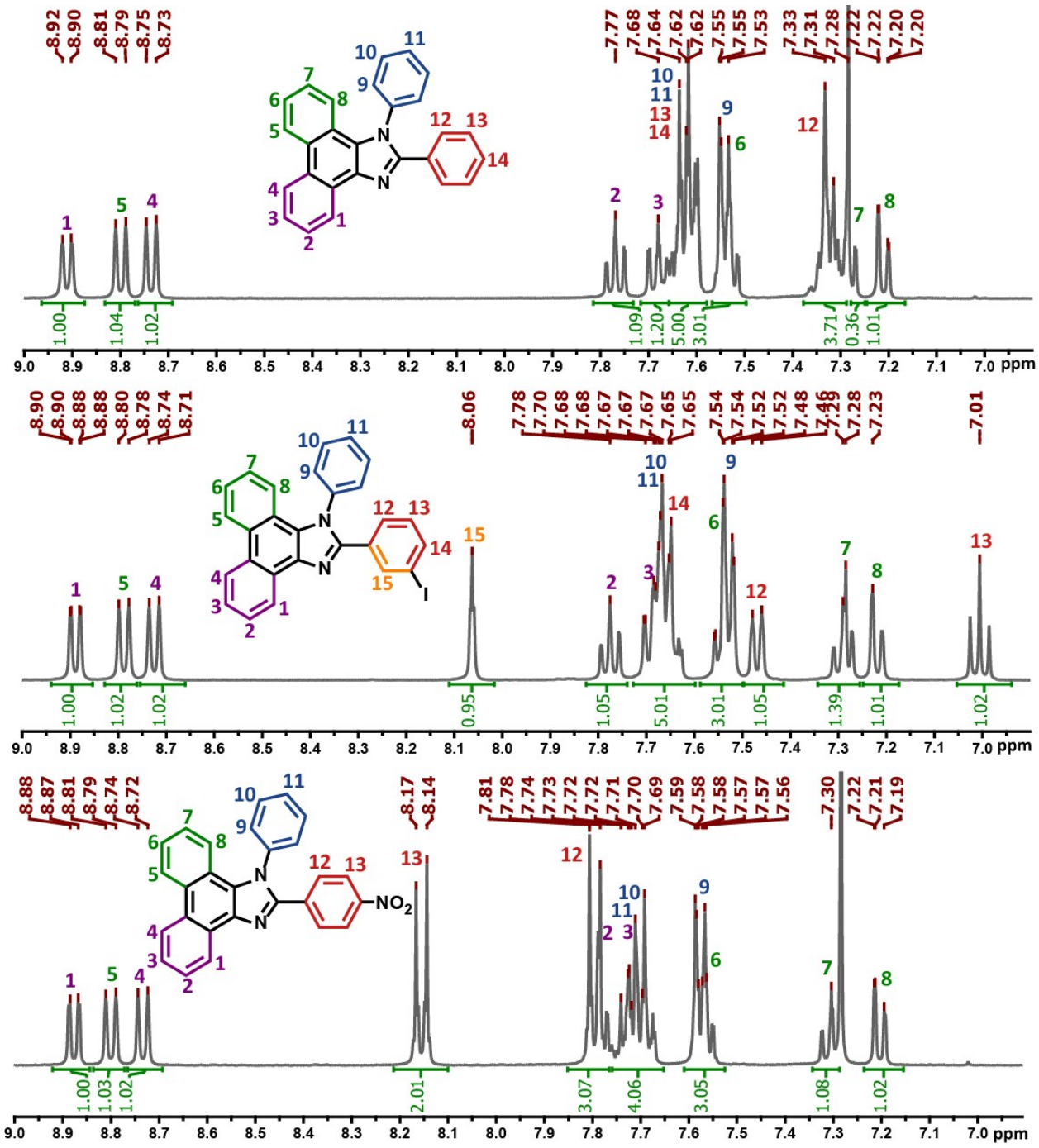

Figure S2. ^{1}H NMR spectra of the ligands in $CDCl_3$, 298 K.

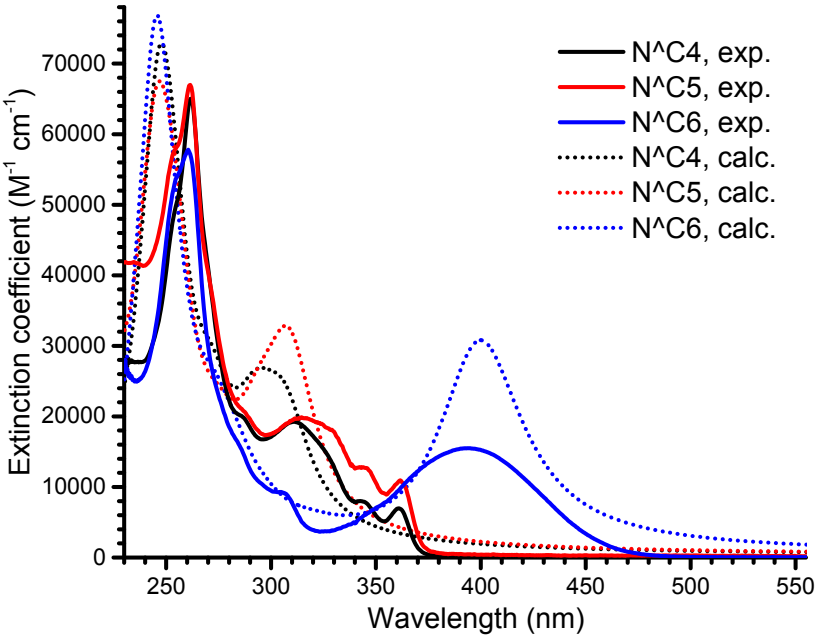

Figure S3. Experimental and calculated absorption spectra for N^C4-N^C6.

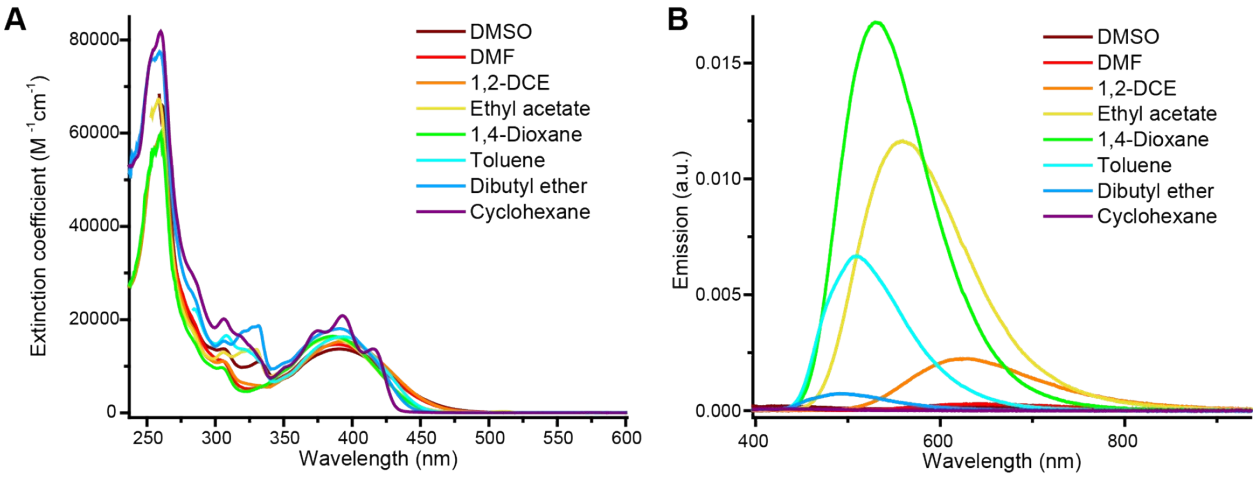

Figure S4. A. Absorption spectra of N^C6 in different solvents, $1*10^{-5}$ M, RT; B. Emission spectra of N^C6 in different solvents, N^C6 = $1\ 10^{-5}$ M, λ_{ex}=365 nm, RT.

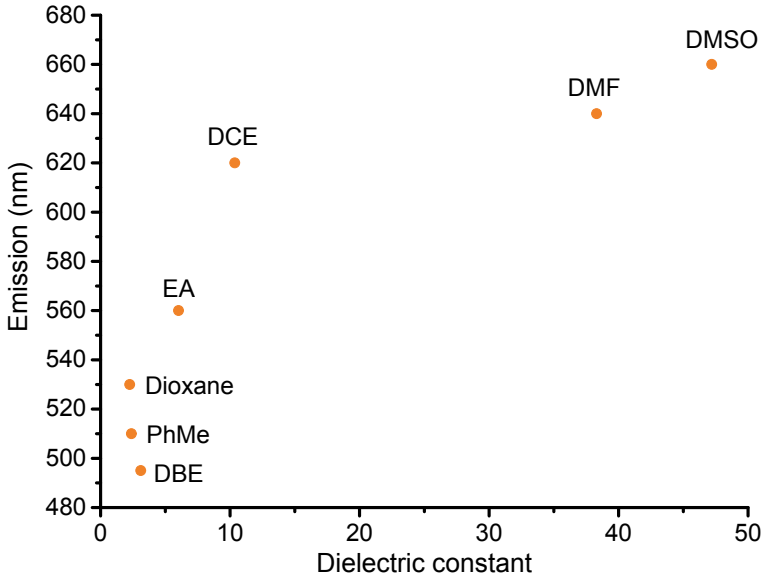

Figure S5. Correlation between emission wavelength of N^C6 and solvent dielectric constant.

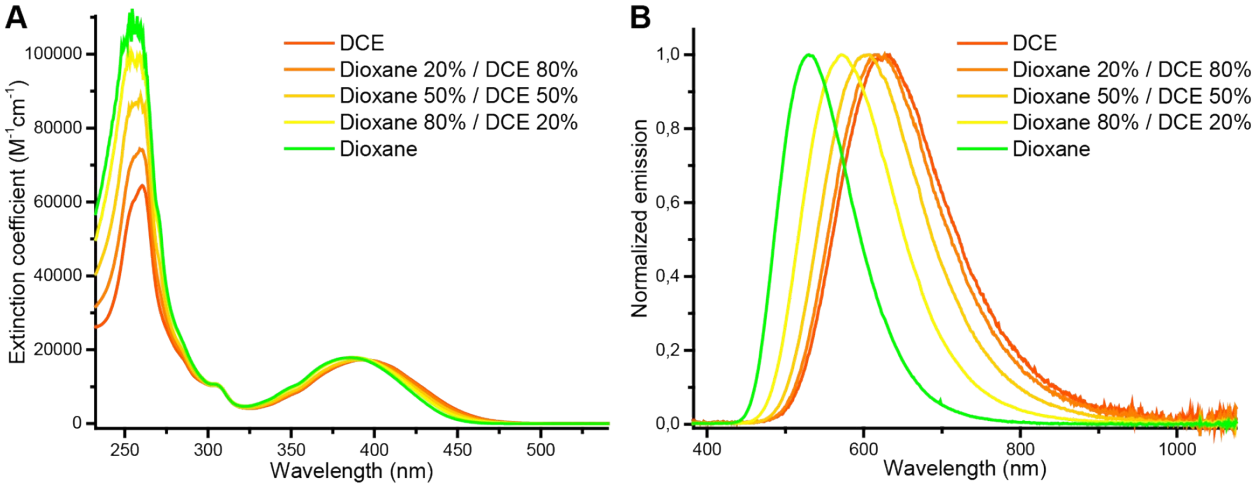

Figure S6. A. Absorption spectra of N^C6 in 1,2-dichloroethane, 1,4-dioxane and their mixtures, c (L6) = 3 10^{-5} M.
*B. Normalized emission spectra of N^C6 in 1,2-dichloroethane, 1,4-dioxane and their mixtures, 3*10^{-5} M, λ_{ex} = 365 nm, RT.*

Table S1. Emission maxima of L6 in different solvents, properties of solvents: dielectric constants and polarity index.

Solvent	$\lambda_{em, nm}$	Dielectric constant, ε	Polarity index	Polarity index 2	$E_t(30)$*
DMSO	660	47.2	7.2	10.00	45.1 (0.444)
DMF	640	38.3	6.4	9.21	43.2 (0.386)
1,2-dichloroethane (DCE)	620	10.36	3.5	8.61	42.3 (0.327)
Ethyl acetate (EA)	560	6.02	4.4	6.96	38.1 (0.228)
1,4-Dioxane (DO)	530	2.25	4.8	5.18	36.0 (0.164)
Toluene	510	2.38	2.4	6.58	33.9 (0.099)
Dibutyl ether (DBE)	495	3.10	2.8 (diethyl ether)	5.5	33.0 (0.071)
Cyclohexane	no emission	2.02	0.2	3.49	30.9 (0.006)

*(C. Reichardt, Chem. Rev., 1994, **94**, 2319–2358.)

Table S2. Charge transfer upon excitation of N^C4-N^C6 in DCE and IFCT tables for the corresponding transitions*.

N^C4, abs., S0→S1,
$\lambda_{calc.}$ = 307 nm, f = 0.289,
main NTO = 86%

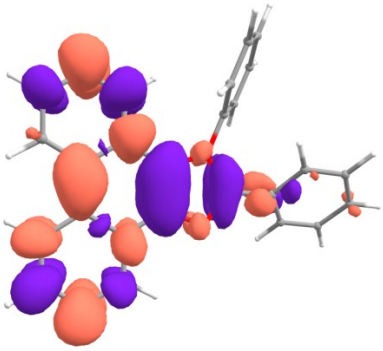

Donor	Acceptor	
	core	Ph
core	0.855	0.081
Ph	0.058	0.006

Net ET to Ph: 0.023

N^C4, abs., S0→S2,
$\lambda_{calc.}$ = 293 nm, f = 0.244,
main NTO = 85%

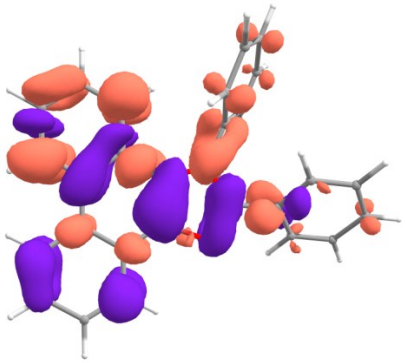

Donor	Acceptor	
	core	Ph
core	0.815	0.103
Ph	0.072	0.009

Net ET to Ph: 0.031

N^C4, abs., S0→S3,
$\lambda_{calc.}$ = 272 nm, f = 0.240,
main NTO = 82%

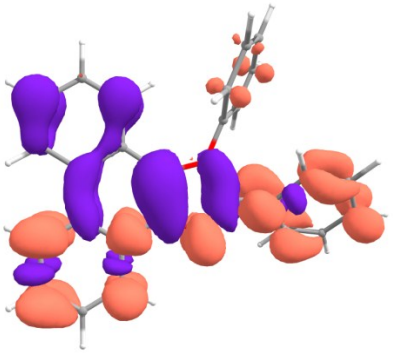

Donor	Acceptor	
	core	Ph
core	0.696	0.209
Ph	0.073	0.022

Net ET to Ph: 0.136

N^C5, abs., S0→S1,
$\lambda_{calc.}$ = 309 nm, f =0.491,
main NTO = 90%

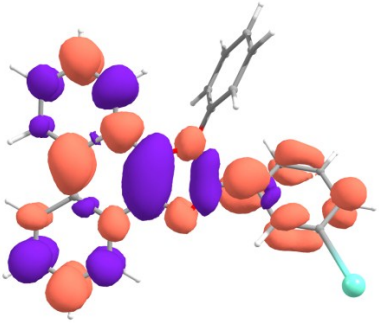

Donor	Acceptor	
	core	m-I-Ph
core	0.736	0.181
m-I-Ph	0.067	0.016

Net ET to m-I-Ph: 0.114

N^C5, abs., S0→S2,
$\lambda_{calc.}$ = 294 nm, f =0.187,
main NTO = 82%

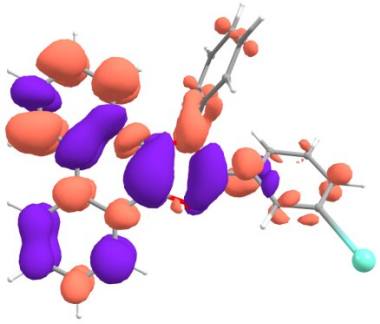

Donor	Acceptor	
	core	m-I-Ph
core	0.819	0.115
m-I-Ph	0.058	0.008

Net ET to m-I-Ph: 0.056

N^C5, abs., S0→S3,
$\lambda_{calc.}$ = 275 nm, f =0.132,
main NTO = 75%

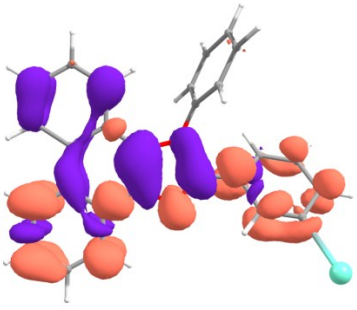

Donor	Acceptor	
	core	m-I-Ph
core	0.672	0.206
m-I-Ph	0.094	0.029

Net ET to m-I-Ph: 0.112

N^C6, abs., S0→S1,
$\lambda_{calc.}$ = 400 nm, f =0.602,
main NTO = 99%

N^C6, abs., S0→S2,
$\lambda_{calc.}$ = 338 nm, f =0.001,
main NTO = 100%

N^C6, abs., S0→S3,
$\lambda_{calc.}$ = 320 nm, f =0.020,
main NTO = 97%

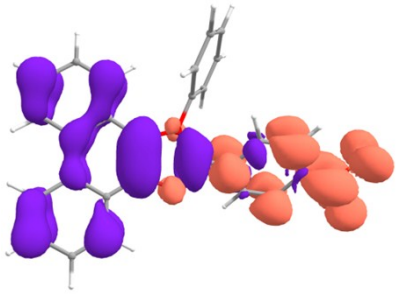

Donor	Acceptor	
	core	pNO_2-Ph
core	0.120	0.728
pNO_2-Ph	0.021	0.130

Net ET to p-NO_2-Ph: 0.707

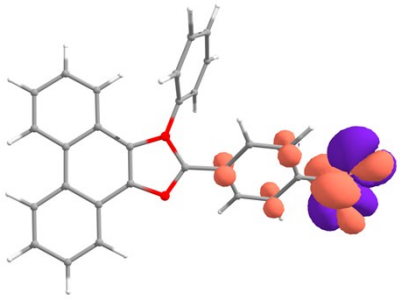

Donor	Acceptor	
	core	pNO_2-Ph
core	0.000	0.000
pNO_2-Ph	0.015	0.989

Net ET to p-NO_2-Ph: -0.015

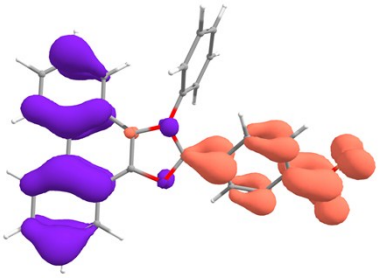

Donor	Acceptor	
	core	pNO_2-Ph
core	0.197	0.795
pNO_2-Ph	0.001	0.005

Net ET to p-NO_2-Ph: 0.795

N^C6H$^+$, abs., S0→S1,
$\lambda_{calc.}$ = 358 nm, f =0.587,
main NTO = 95%

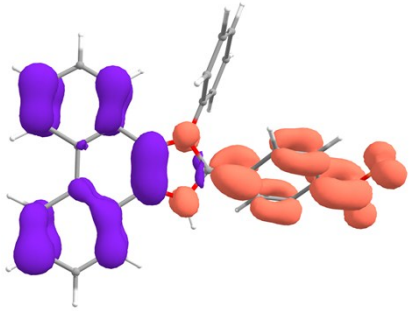

Donor	Acceptor	
	core	pNO_2-Ph
core-H$^+$	0.272	0.672
pNO_2-Ph	0.016	0.040

Net ET to p-NO_2-Ph: 0.656

N^C6H$^+$, abs., S0→S2,
$\lambda_{calc.}$ = 340 nm, f =0.012,
main NTO = 94%

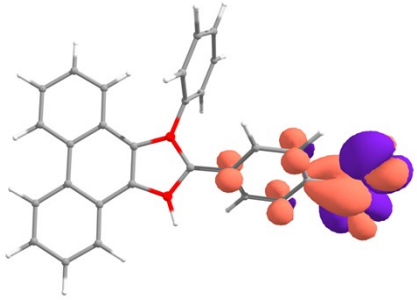

Donor	Acceptor	
	core	pNO_2-Ph
core-H$^+$	0.000	0.008
pNO_2-Ph	0.037	0.955

Net ET to p-NO_2-Ph: -0.029

N^C6H$^+$, abs., S0→S3,
$\lambda_{calc.}$ = 319 nm, f =0.014,
main NTO = 97%

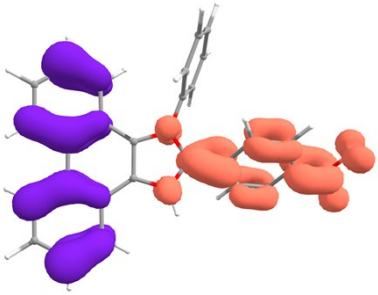

Donor	Acceptor	
	core	pNO_2-Ph
core-H$^+$	0.307	0.693
pNO_2-Ph	0.000	0.000

Net ET to p-NO_2-Ph: 0.693

Table S3. Charge transfer upon emission of N^C4-N^C6 and -N^C6H$^+$ in DCE and IFCT tables for S1→S0 transition*.

N^C4, em., S1→S0, 383 nm

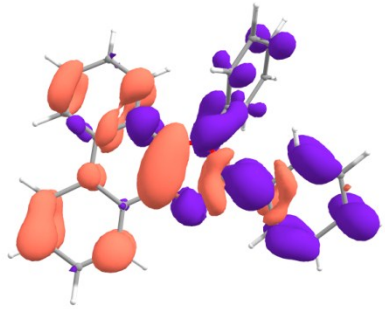

Donor	Acceptor	
	core	Ph
core	0.524	0.286
Ph	0.123	0.067

Net ET from Ph: 0.163

N^C5, em., S1→S0, 389 nm

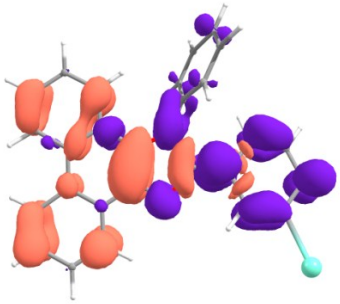

Donor	Acceptor	
	core	m-I-Ph
core	0.479	0.100
m-I-Ph	0.348	0.073

Net ET from m-I-Ph: 0.248

N^C6, em., S1→S0, 511 nm

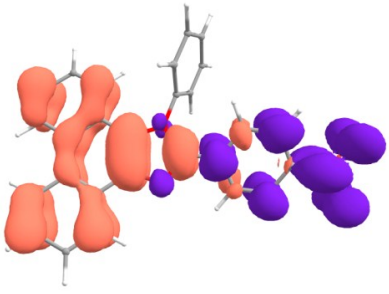

Donor	Acceptor	
	core	pNO2-Ph
core	0.103	0.014
pNO_2-Ph	0.776	0.107

Net ET from pNO_2-Ph: 0.762

N^C6H$^+$, em., S0→S1, 477 nm

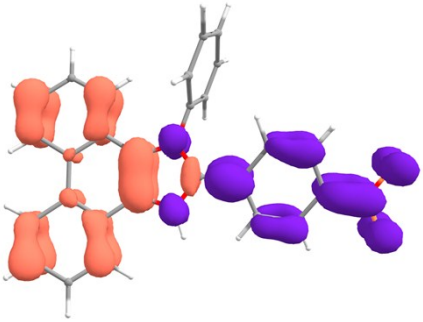

Donor	Acceptor	
	core-H^+	pNO_2-Ph
core-H^+	0.288	0.040
pNO_2-Ph	0.590	0.082

Net ET to p-NO_2-Ph: 0.550

* The figures show variations in electronic density upon excitation and emission. Violet and terracotta are depletion and increase of electronic density, respectively. Main NTO is contibution of main NTO couple into transition. The data for the corresponding interfragment charge transfer (IFCT) are given below the figures. Diagonal values represent intraligand transitons, off-diagonal values represent a charge transfer from "Donor" to "Acceptor". Core - phenanthro-imidazole fragment, Ph – phenyl, m-I-Ph – m-iodophenyl, p-NO_2-Ph – p-nitrophenyl. Net electron transfer (Net ET) values, calculated from IFCT.

Table S4. Experimental and calculated values for low energy absorption and emission for N^C4-N^C6, including the data for N^C6 in different solvents.

Ligand (Solvent)	λ_{abs} (exp.) nm	λ_{abs} (calc.) nm	λ_{em} (exp.) nm	λ_{em} (calc. PCM model) nm	N^C6 + 1 solvent λ_{em} (calc.) nm	N^C6 + 2 solvent λ_{em} (calc.) nm	N^C6 +3 solvent λ_{em} (calc.) nm	N^C6 + 4 solvent λ_{em} (calc.) nm
N^C4 (DCE)	361	307	370	383	–	–	–	–
N^C5 (DCE)	361	309	370	389	–	–	–	–
N^C6 (DCE)	390	400	620	511	517	528		538
N^C6H$^+$ (DCE)	356	356	586	477	–	–	–	–
N^C6 (Cyclohexane)	416	391	–*	460	–	–	–	–
N^C6 (Diethyl ether)	392**	396	495**	489	–	–	–	–
N^C6 (DMSO)	392	401	660	528	541	570	588	595
N^C6 (Toluene)	394	393	510	467	480	500		
N^C6 (1,4-Dioxane)	386	391	530	464	475	482	508	520
N^C6 (Ethyl acetate)	386	398	560	499	508			

* — no emission; ** — in dibutyl ether.

The crystal structures of **1**, **2**, **4-6** and **N^C6** were determined by the means of single crystal X-ray diffraction analysis. Crystals were fixed on a micro mounts and the diffraction data have been collected on the various Rigaku Oxford Diffraction diffractometers at a temperature of 100K. Crystals of **1** and **N^C6** were placed on the Excalibur Eos diffractometer and measured using monochromated Mo*Kα* radiation. Crystal of **2** was placed on the SuperNova Atlas diffractometer and measured using monochromated microfocused Cu*Kα* radiation. Crystals of **4-6** were placed on XtaLAB HyPix-3000 diffractometer and measured using monochromated microfocused Cu*Kα* radiation. Data were integrated and corrected for background, Lorentz, and polarization effects. An empirical absorption correction based on spherical harmonics implemented in the SCALE3 ABSPACK algorithm was applied in *CrysAlisPro* program.[37] The unit-cell parameters (Tables S6) were refined by the least-squares techniques. The structures

were solved by direct methods or dual-space algorithm and refined using the *SHELX* programs[38,39] incorporated in the *OLEX2* program package.[40] The final models included coordinates and anisotropic displacement parameters for all non-H atoms. The carbon and nitrogen-bound H atoms were placed in calculated positions and were included in the refinement in the 'riding' model approximation, U_{iso}(H) set to 1.5U_{eq}(C) and C–H 0.96 Å for the CH_3 groups, U_{iso}(H) set to 1.2U_{eq}(C) and C–H 0.97 Å for the CH_2 groups, U_{iso}(H) set to 1.2U_{eq}(C) and C–H 0.93 Å for the CH groups of the cyclic fragments, and U_{iso}(H) set to 1.2U_{eq}(C) and C–H 0.98 Å for the tertiary CH groups. The unit cells of **4-6** contain disordered solvent molecules which have been treated as a diffuse contribution to the overall scattering without specific atom positions by SQUEEZE/PLATON.[41] The total Potential Solvent Accessible Void Vol in **4** is 444 Å^3 and electron Count Voids / Cell = 98 that is approximately equal to 1 acetone molecule per formula unit. The total Potential Solvent Accessible Void Vol in **5** is 3033 Å^3 and electron Count Voids / Cell = 893 that is approximately equal to 1 chloroform and 1 diethyl ether molecule per formula unit. The total Potential Solvent Accessible Void Vol in **6** is 779 Å^3 and electron Count Voids / Cell = 94 that is approximately equal to 0.5 acetonitrile molecules per formula unit. The crystal structures of **2** and **N^C6** were refined as an inversion twins. Supplementary crystallographic data for this paper have been deposited at Cambridge Crystallographic Data Centre (CCDC 1964885 - 1964890) and can be obtained free of charge via www.ccdc.cam.ac.uk/structures/.

Table S5. Selected bond distances (Å) and angles (°).

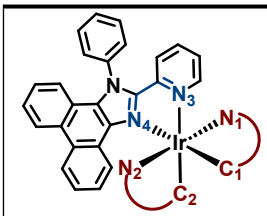	**1**	**2**	**4**	**5**	**6**
Distances, Å					
Ir-C1	1.998(3)	2.014(10)	1.996(5)/1.988(5)	2.008(10)	2.000(3)
Ir-N1	2.035(3)	2.043(8)	2.093(4)/2.079(5)	2.104(7)	2.120(2)
Ir-C2	2.018(3)	2.014(10)	2.031(5)/2.009(5)	2.036(10)	2.034(2)
Ir-N2	2.051(3)	2.069(8)	2.075(4)/2.080(5)	2.098(7)	2.100(2)
Ir-N3	2.166(3)	2.147(9)	2.137(5)/2.167(4)	2.210(6)	2.161(2)
Ir-N4	2.242(3)	2.199(8)	2.258(4)/2.320(4)	2.282(7)	2.294(2)
Angles, °					
N1-Ir-C1	80.75(12)	80.3(4)	80.65(19)/79.7(2)	79.8(3)	79.65(9)
N2-Ir-C2	80.53(12)	79.9(4)	79.30(19)/79.88(19)	79.7(3)	79.53(9)
N3-Ir-N4	75.28(10)	76.2(3)	74.53(16)/74.68(15)	75.3(2)	74.85(8)
C1-Ir-C2	84.52(13)	85.3(4)	86.9(2)/88.8(2)	84.3(3)	83.94(9)
C2-Ir-N1	93.45(12)	98.9(4)	94.24(19)/92.0(2)	91.5(4)	92.88(9)
C2-Ir-N4	107.73(11)	102.3(3)	100.86(18)/103.09(18)	105.2(3)	101.94(9)
C1-Ir-N2	95.47(12)	96.5(4)	92.25(19)/94.0(2)	93.9(3)	93.04(9)
N2-Ir-N4	88.32(10)	87.4(3)	80.00(16)/79.69(16)	78.9(3)	77.32(7)
N4-Ir-N1	96.54(10)	95.9(3)	107.98(16)/108.25(16)	108.9(3)	110.83(7)
N3-Ir-N2	97.36(10)	95.5(3)	98.55(17)/103.67(17)	107.4(3)	104.32(8)
N3-Ir-N1	88.47(10)	85.8(3)	88.37(17)/84.81(17)	81.5(3)	83.78(8)
N3-Ir-C1	92.55(11)	96.3(4)	97.47(18)/94.08(19)	96.5(3)	100.21(9)

Table S6. Crystallographic data for 1, 2, 4, 5, 6 and N^C6.

Compound	**1**	**2**	**4**	**5**	**6**	**N^C6**
Formula	$C_{48}H_{33}IrN_5$, (C HCl_3)$_3$, PF_6	$C_{52}H_{33}IrN_5S_2$, (C_4 $H_{10}O$)$_{2.13}$, (CH_2Cl_2)$_{0.75}$, PF_6	$C_{80}H_{51}IrN_7$, PF_6, ($CHCl_3$)$_{0.13}$, (C_3H_6O)$_{0.25}$	$C_{80}H_{49}I_2IrN_7$, PF_6	$C_{80}H_{49}IrN_9O_4$, PF_6, ($C_4H_{10}O$)$_{0.5}$	$C_{27}H_{17}N_3O_2$
Crystal System	Monoclinic	Orthorhombic	Triclinic	Monoclinic	Monoclinic	Orthorhombic
a (Å)	13.7115(2)	35.6730(5)	17.5554(2)	52.252(2)	30.2713(6)	27.1016(9)
b (Å)	18.8612(3)	33.4826(5)	20.8344(3)	13.6314(4)	15.7377(2)	11.3994(5)
c (Å)	21.0299(4)	19.7402(2)	21.1839(4)	23.8081(9)	31.0641(6)	6.2796(3)
α (°)	90	90	61.714(2)	90	90	90
β (°)	108.308(2)	90	86.958(1)	120.633(5)	113.642(2)	90
γ (°)	90	90	82.312(1)	90	90	90
V (Å^3)	5163.36(16)	23578.1(6)	6761.2(2)	14591.3(11)	13556.9(5)	1940.03(14)
Molecular weight	1375.07	1350.32	1476.89	1699.23	1574.51	415.43
Space group	$P2_1/n$	$Fdd2$	$P\bar{1}$	$C2/c$	$C2/c$	$Pna2_1$
μ (mm^{-1})	3.147	6.489	4.745	10.916	4.697	0.092
Temperature (K)	100(2)	100(2)	100(2)	100(2)	100(2)	100(2)
Z	8	16	4	8	8	2
D_{calc} (g/cm^3)	1.769	1.522	1.451	1.547	1.543	1.422
Crystal size (mm^3)	0.21 × 0.17 × 0.11	0.18 × 0.12 × 0.09	0.37 × 0.23 × 0.02	0.30 × 0.06 × 0.02	0.08 × 0.05 × 0.02	0.19 × 0.02 × 0.01
Diffractometer	Xcalibur Eos	SuperNova Atlas	XtaLAB HyPix-3000	SuperNova Atlas	XtaLAB HyPix-3000	Xcalibur Eos
Radiation	Mo$K\alpha$	Cu$K\alpha$	Cu$K\alpha$	Cu$K\alpha$	Cu$K\alpha$	Mo$K\alpha$
Total reflections	52304	117136	25580	13113	12833	19264
Unique reflections	11856	11113	25580	13113	12833	4446
Angle range 2θ (°)	5.33–55.00	5.76–140.00	4.74–140.00	6.78–140.00	6.37–140.00	5.75–55.00
Reflections with $\|F_o\| \geq 4\sigma_F$	10295	10878	21537	7432	12011	4014
R_{int}	0.0408	0.0779	Merged	Merged	Merged	0.0515
R_σ	0.0335	0.0288	0.0359	0.1009	0.0192	0.0478
R_1 ($\|F_o\| \geq 4\sigma_F$)	0.0304	0.0610	0.0560	0.0617	0.0266	0.0435
wR_2 ($\|F_o\| \geq 4\sigma_F$)	0.0697	0.1578	0.1619	0.1420	0.0679	0.0898
R_1 (all data)	0.0384	0.0617	0.0651	0.1034	0.0287	0.0513
wR_2 (all data)	0.0751	0.1590	0.1687	0.1576	0.0691	0.0935
S	1.043	1.067	1.075	0.898	1.037	1.058
ρ_{min}, ρ_{max}, *e*/Å^3	–1.503, 1.937	–1.569, 2.012	–2.832, 3.292	–1.309, 1.262	–0.976, 1.044	–0.234, 0.267
CCDC	1964885	1964886	1964887	1964888	1964889	1964890

$R_1 = \Sigma||F_o| - |F_c||/\Sigma|F_o|$; $wR_2 = \{\Sigma[w(F_o^2 - F_c^2)^2]/\Sigma[w(F_o^2)^2]\}^{1/2}$; $w = 1/[\sigma^2(F_o^2)+(aP)^2 + bP]$, where $P = (F_o^2 + 2F_c^2)/3$; $s = \{\Sigma[w(F_o^2 - F_c^2)]/(n - p)\}^{1/2}$ where *n* is the number of reflections and *p* is the number of refinement parameters.

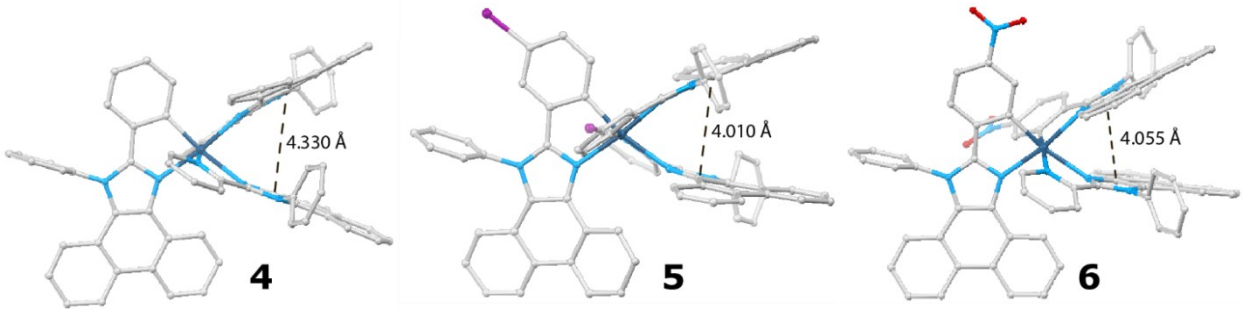

Figure S7. Intramolecular π-π interaction in the solid state structure of 4-6.

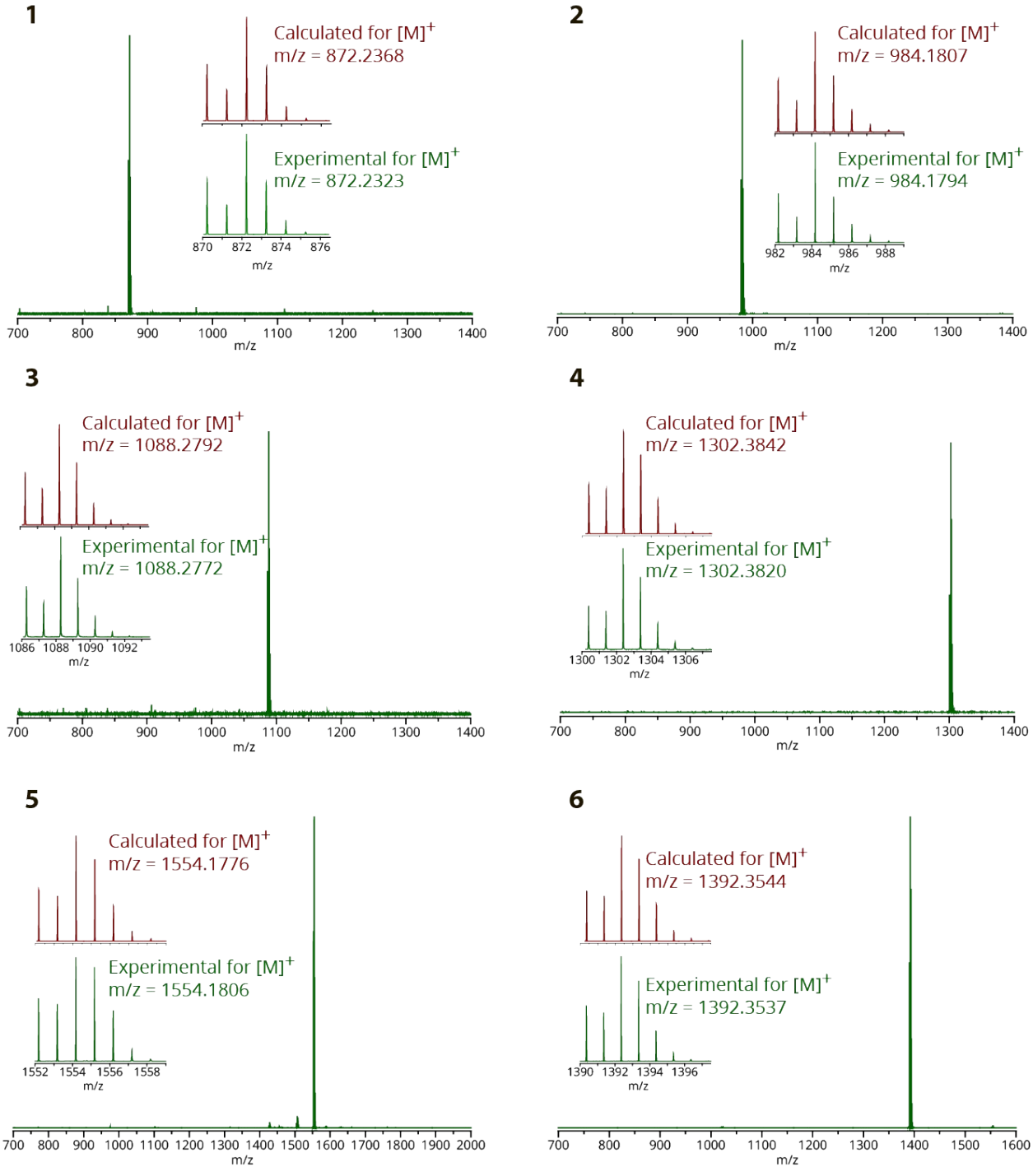

Figure S8. Experimental and calculated ESI+ mass spectra of 1-6.

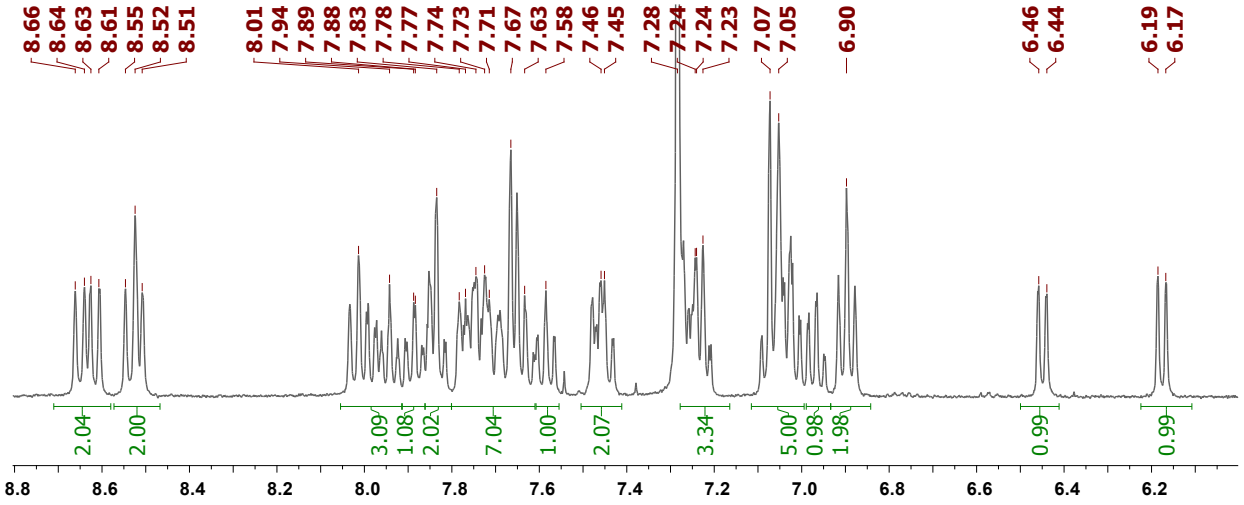

Figure S9. ^1H NMR spectrum of 1 in $CDCl_3$, 298 K.

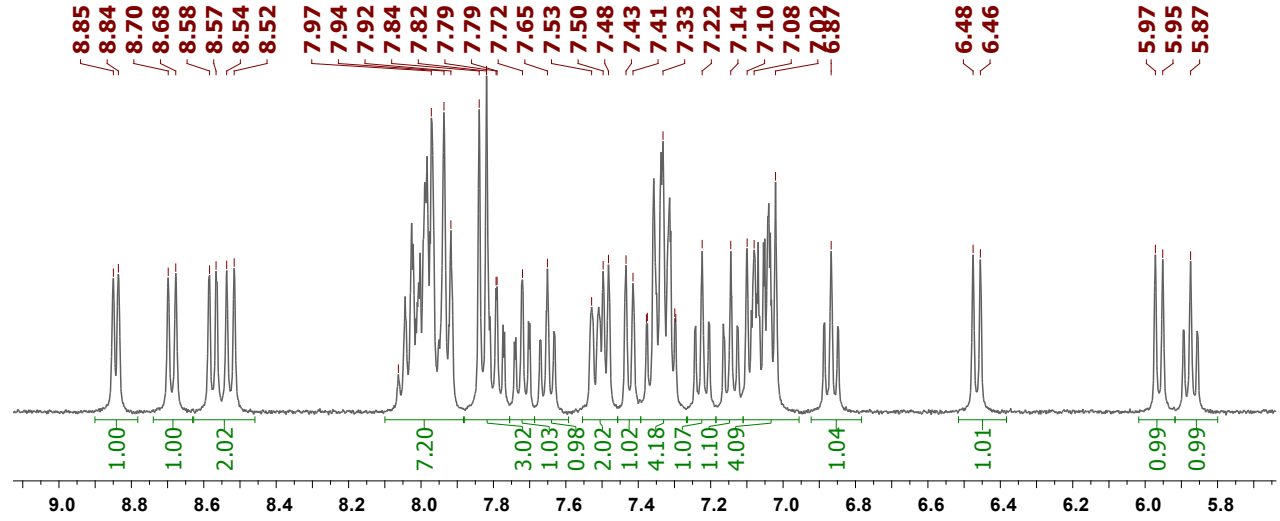

Figure S10. ^1H NMR spectrum of 2 in CD_2Cl_2, 298 K.

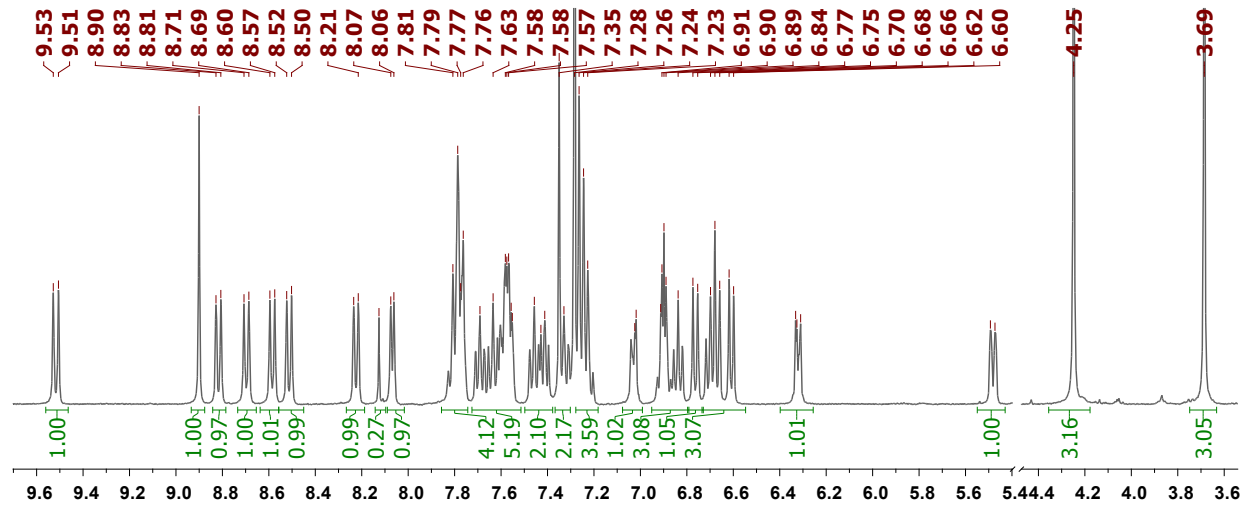

Figure S11. ^1H NMR spectrum of 3 in $CDCl_3$, 298 K.

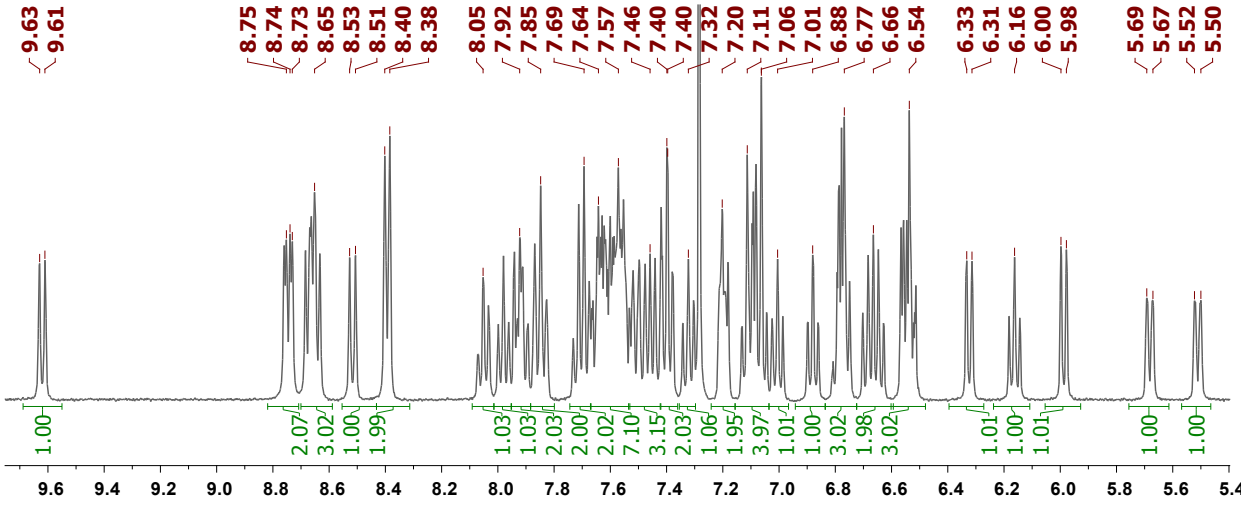

Figure S12. ^1H NMR spectrum of 4 in $CDCl_3$, 298 K.

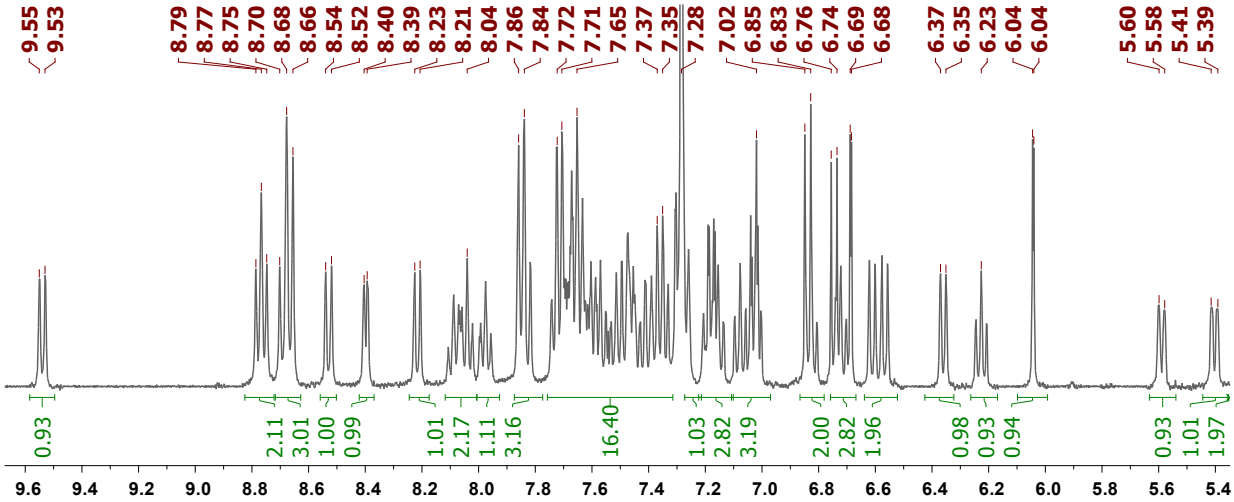

Figure S13. ^1H NMR spectrum of 5 in $CDCl_3$, 298 K.

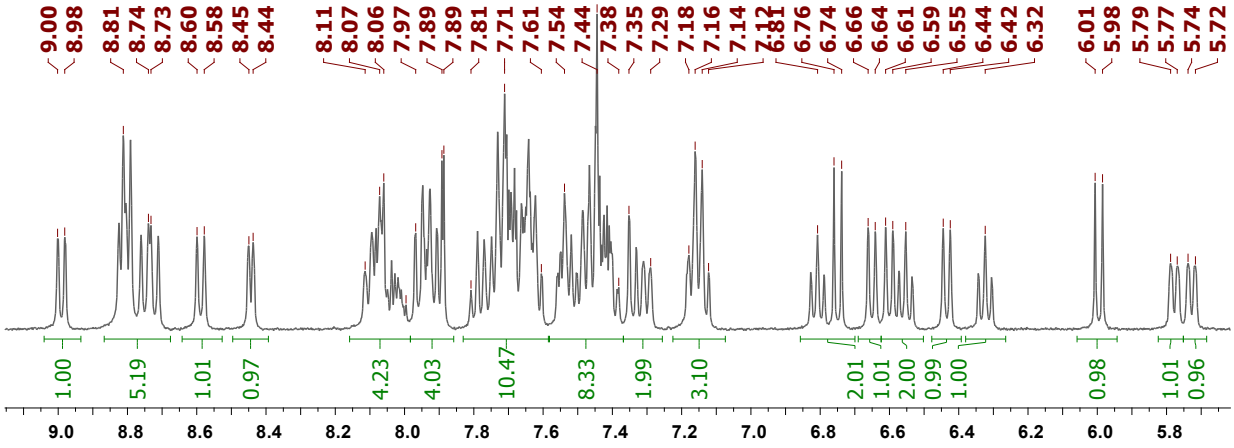

Figure S14. ^1H NMR spectrum of 6 in CD_2Cl_2, 298 K.

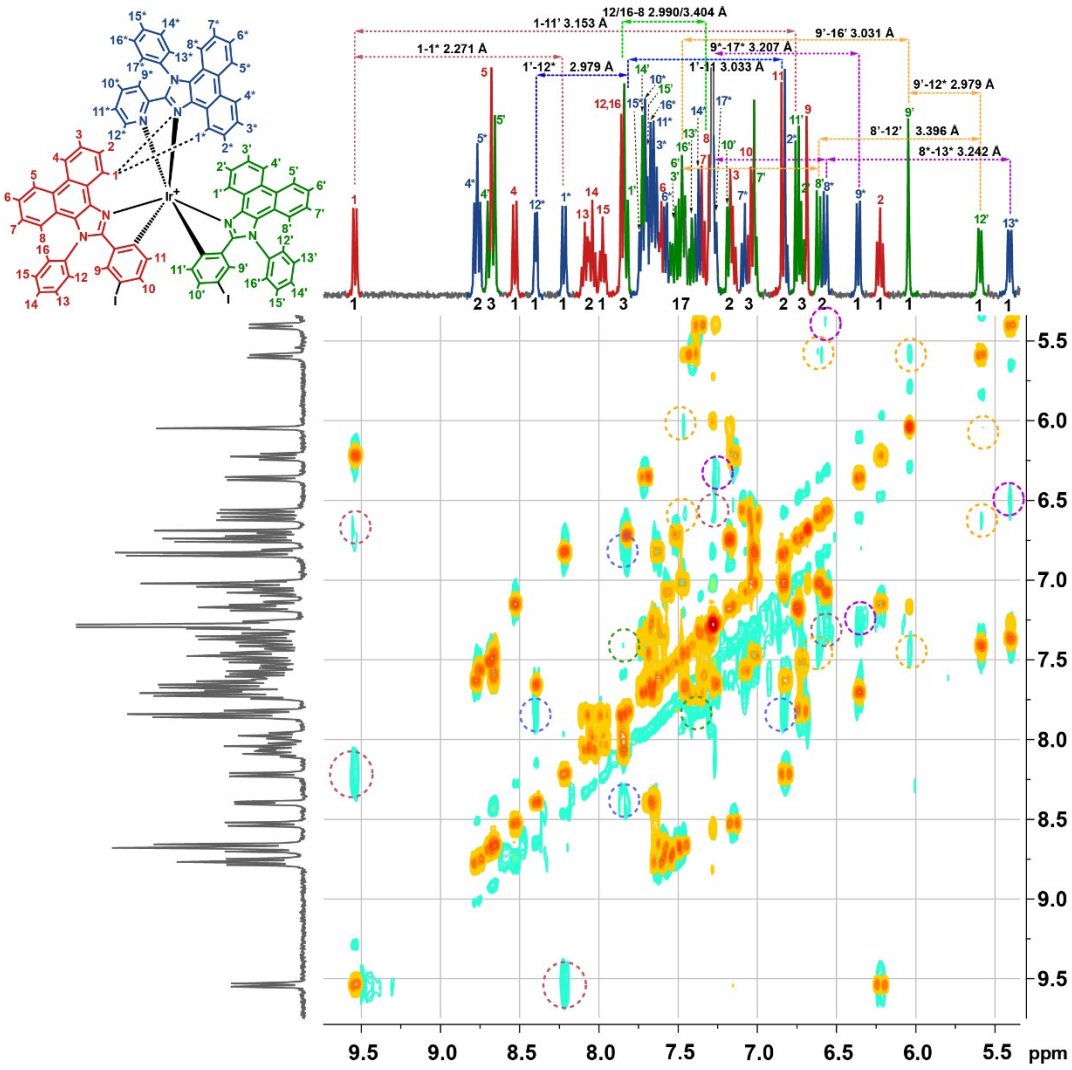

Figure S15. Overlapped ^{1}H-^{1}H COSY and NOESY NMR spectra of 5 with full assignment of the signals. Top-left structure of the complex shows atom numbering scheme, short contacts between protons revealed in the NOESY spectrum are also accompanied with the distances found in solid state structure.

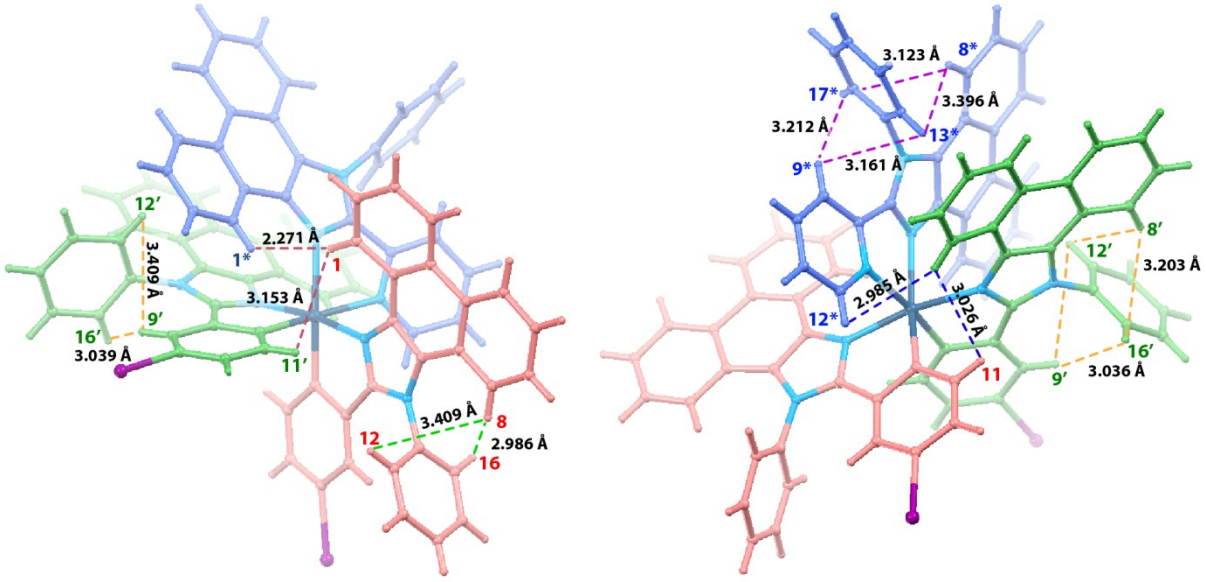

Figure S16. **Intramolecular short proton-proton contacts in 5 in the solid state.**

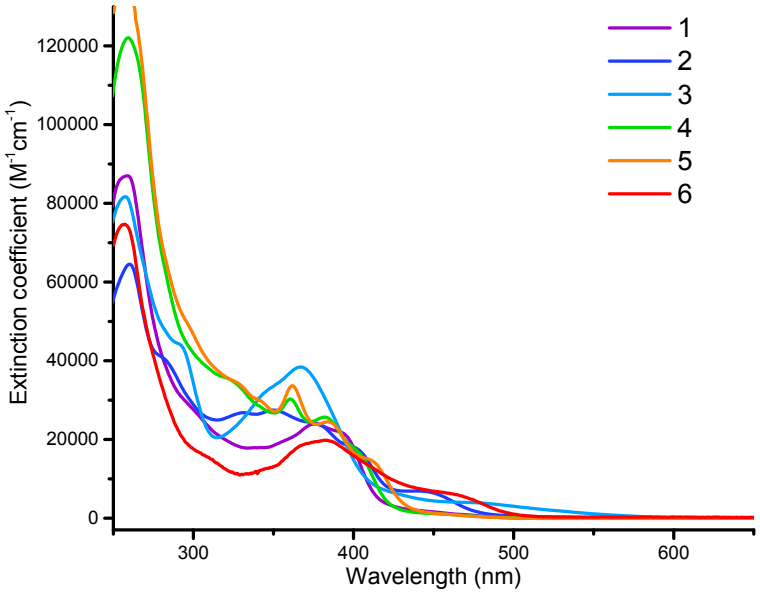

Figure S17. Absorption spectra of 1-6 in CH_2Cl_2 ($1*10^{-5}$ M).

Computational results for iridium complexes 1-6

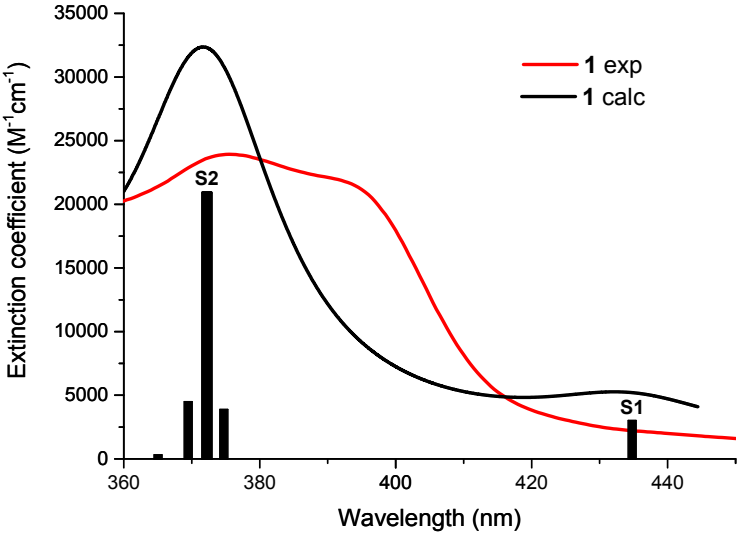

Figure S18. **Experimental and calculated absorption spectra of 1. Line halfwidth in the calculated spectrum is 900 cm^{-1}.**

Table S7. Experimental and calculated data for absorption spectrum of 1. Wavelength (λ), extinction coefficients (ε), oscillator strengths (f) and NTO contribution in the corresponding transition.

λ, nm (exp)	ε*10^{-3}, M^{-1} cm^{-1} (exp)	Transitions	λ, nm (calc)	*f* (calc)	Contribution of main NTO in transition, %
445sh	1.7	$S_0 \rightarrow S_1$	435	0.0373	97
375	24	$S_0 \rightarrow S_2$	372	0.2555	77

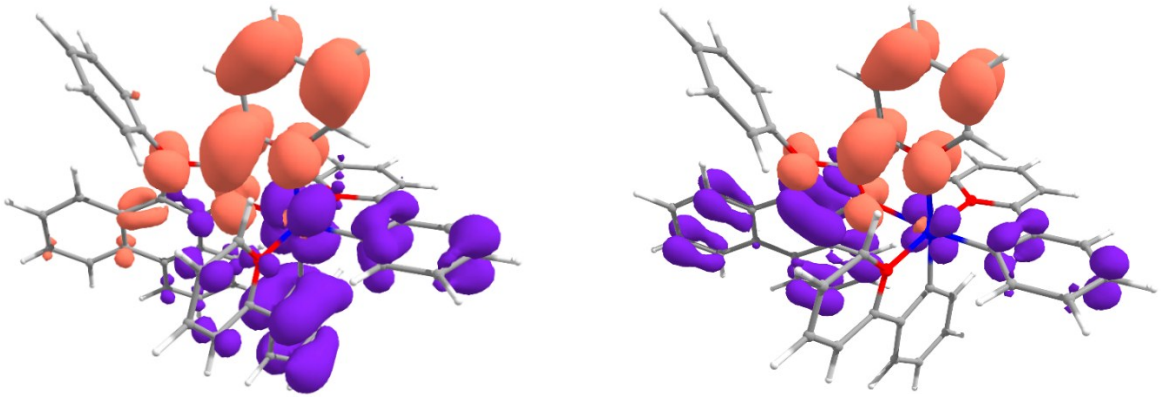

Figure S19. Variations in electronic density upon absorption transitions $S_0 \rightarrow S_i$ (i=1-2) of 1. Violet and terracotta denote decrease and increase of electron density, respectively.

Table S8. IFCT for electronic transitions S_0-S_1 and S_0-S_2.

S_0-S_1					S_0-S_2				
Donor	Acceptor				Donor	Acceptor			
	Ir	N^N	N^C1	N^C2		Ir	N^N	N^C1	N^C2
Ir	0.01	0.24	0.01	0	Ir	0	0.06	0.01	0.02
N^N	0.01	0.17	0	0	N^N	0.02	0.57	0.02	0.02
N^C1	0.01	0.33	0.01	0	N^C1	0	0.04	0.01	0.02
N^C2	0	0.16	0	0	N^C2	0	0.12	0.01	0.01

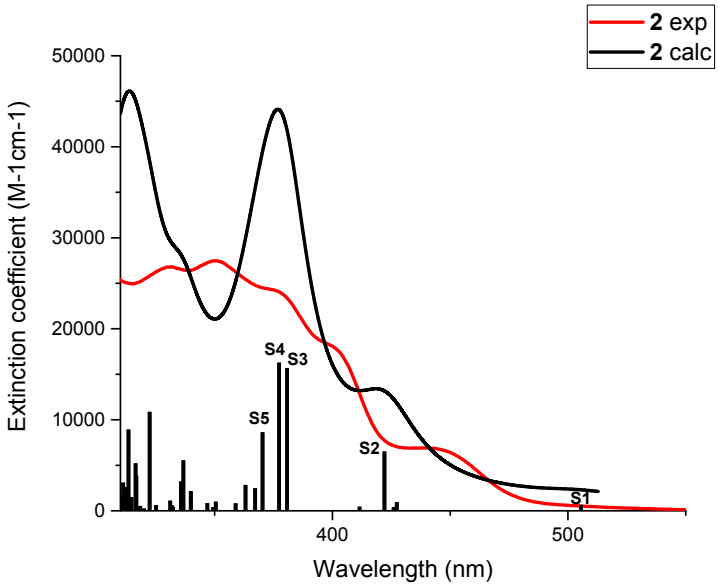

Figure S20. Experimental and calculated absorption spectra of 2. Line halfwidth in the calculated spectrum is 900 cm^{-1}.

Table S9. Experimental and calculated data for absorption spectrum of 2. Wavelength (λ), extinction coefficients (ε), oscillator strengths (f) and NTO contribution in the corresponding transition.

λ, nm (exp)	ε*10^{-3}, M^{-1} cm^{-1} (exp)	Transitions	λ, nm (calc)	*f* (calc)	Contribution of main NTO in transition, %
500sh (ex)	-	$S_0 \rightarrow S_1$	505	0.0072	99
435sh	7	$S_0 \rightarrow S_2$	422	0.079	93
370sh	24	$S_0 \rightarrow S_3$	381	0.1907	51
		$S_0 \rightarrow S_4$	377	0.1981	48

		$S_0 \rightarrow S_5$	370	0.1047	92

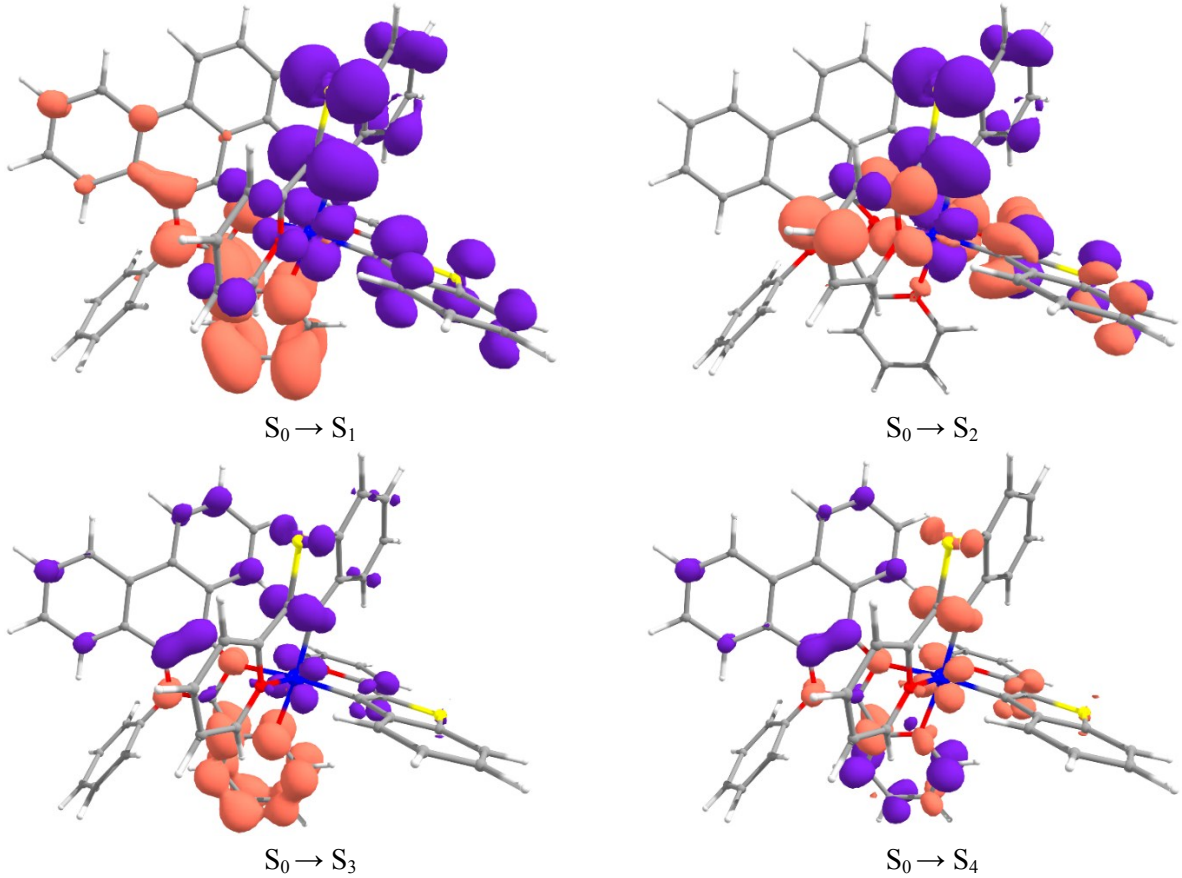

Figure S21. Variations in electronic density upon absorption transitions $S_0 \rightarrow S_i$ (i=1-4) of 2. Violet and terracotta denote decrease and increase of electron density, respectively.

Table S10. Interfragment charge transfer (IFCT) for electronic transitions in 2.

S_0-S_1					S_0-S_2				
Donor	Acceptor				Donor	Acceptor			
	Ir	N^N	N^C1	N^C2		Ir	N^N	N^C1	N^C2
Ir	0	0.16	0	0	Ir	0.01	0.02	0.09	0.05
N^N	0	0.04	0	0	N^N	0	0.01	0.02	0.01
N^1C	0.01	0.29	0	0.01	N^1C	0.01	0.05	0.16	0.09
N2^C	0.01	0.44	0.01	0.01	N2^C	0.02	0.06	0.24	0.13
S_0-S_3					S_0-S_4				
Donor	Acceptor				Donor	Acceptor			
	Ir	N^N	N^C1	N^C2		Ir	N^N	N^C1	N^C2
Ir	0	0.07	0.01	0.01	Ir	0	0.07	0.01	0.01
N^N	0.01	0.46	0	0.01	N^N	0.01	0.41	0.01	0.01
N^C1	0	0.12	0.01	0.02	N^C1	0	0.12	0.02	0.03
N^C2	0	0.2	0.02	0.03	N^C2	0	0.2	0.02	0.03

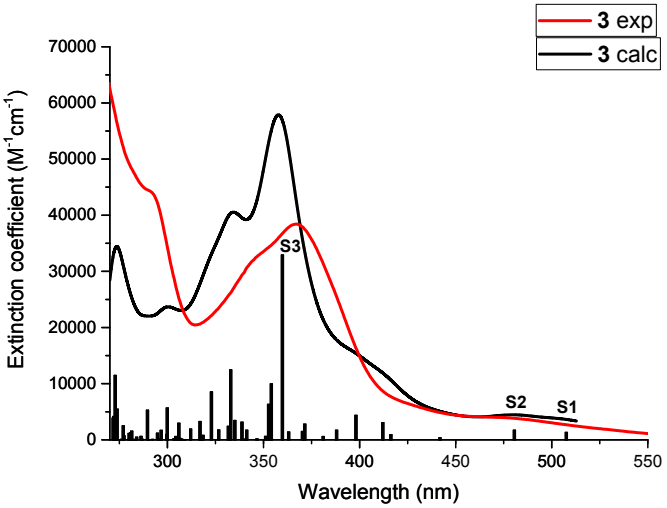

Figure S22. Experimental and calculated absorption spectra of 3. Line halfwidth in the calculated spectrum is 900 cm^{-1}.

Table S11. Experimental and calculated data for absorption spectrum of 3. Wavelength (λ), extinction coefficients (ε), oscillator strengths (f) and NTO contribution in the corresponding transition.

λ, nm (exp)	ε*10^{-3}, M^{-1} cm^{-1} (exp)	Transitions	λ, nm (calc)	*f* (calc)	Contribution of main NTO in transition, %
-	-	$S_0 \rightarrow S_1$	507	0.0171	98
465sh	4.1	$S_0 \rightarrow S_2$	403	0.022	98
367	38	$S_0 \rightarrow S_3$	371	0.1358	59

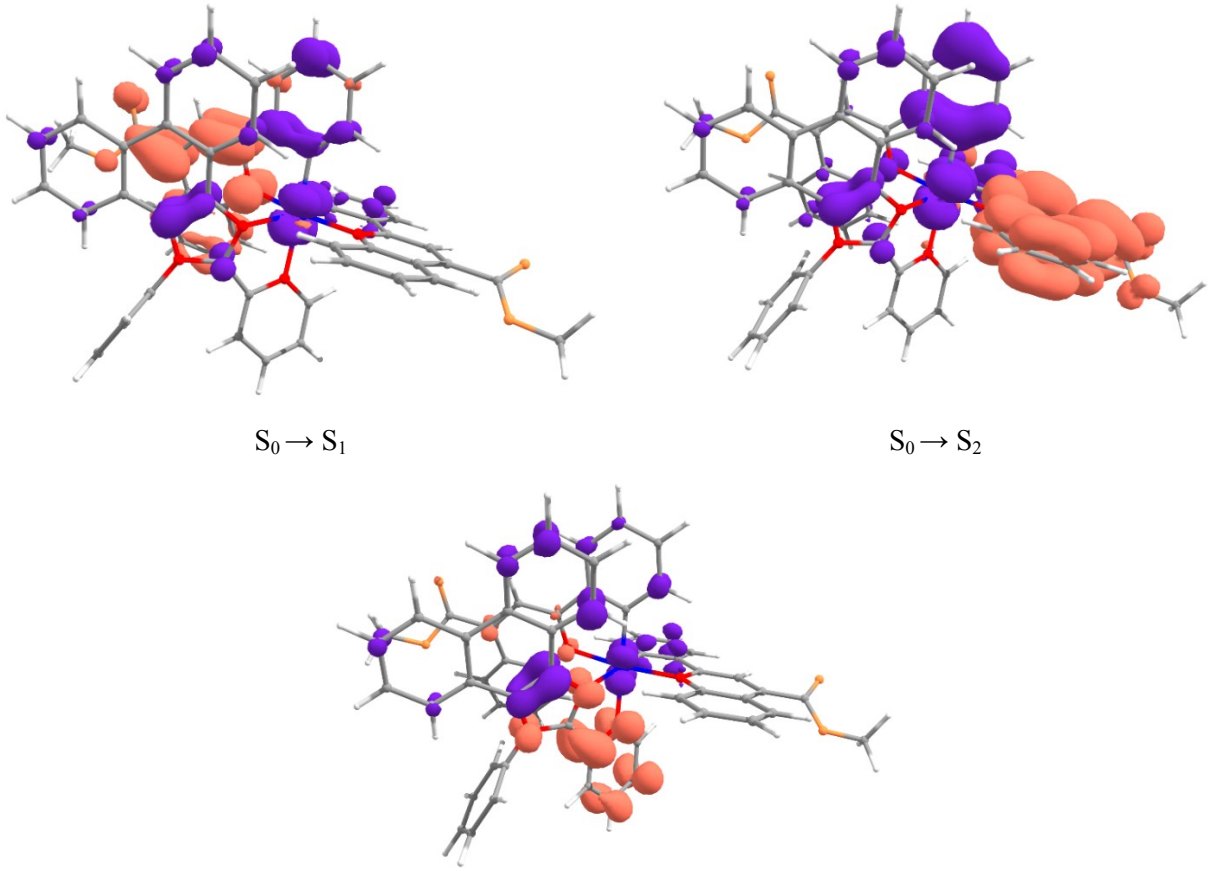

$S_0 \rightarrow S_1$ $S_0 \rightarrow S_2$

$S_0 \rightarrow S_3$

Figure S23. Variations in electronic density upon absorption transitions $S_0 \rightarrow S_i$ (i=1-3) of 3. Violet and terracotta denote decrease and increase of electron density, respectively.

Table S12. Interfragment charge transfer (IFCT) for electronic transitions in 3.

S_0-S_1					S_0-S_2					S_0-S_3				
Donor	Acceptor				Donor	Acceptor				Donor	Acceptor			
	Ir	N^N	N^C1	N^C2		Ir	N^N	N^C1	N^C2		Ir	N^N	N^C1	N^C2
Ir	0.01	0	0	0.20	Ir	0	0.06	0.04	0.01	Ir	0.02	0.03	0.02	0.02
N^N	0.01	0.01	0	0.31	N^N	0.01	0.35	0.03	0.01	N^N	0.05	0.11	0.06	0.06
N^C1	0.01	0	0	0.28	N^1C	0.01	0.04	0.1	0.03	N^C1	0.05	0.13	0.07	0.07
N^C2	0.01	0	0	0.14	N2^C	0.01	0.12	0.09	0.03	N^C2	0.06	0.13	0.07	0.07

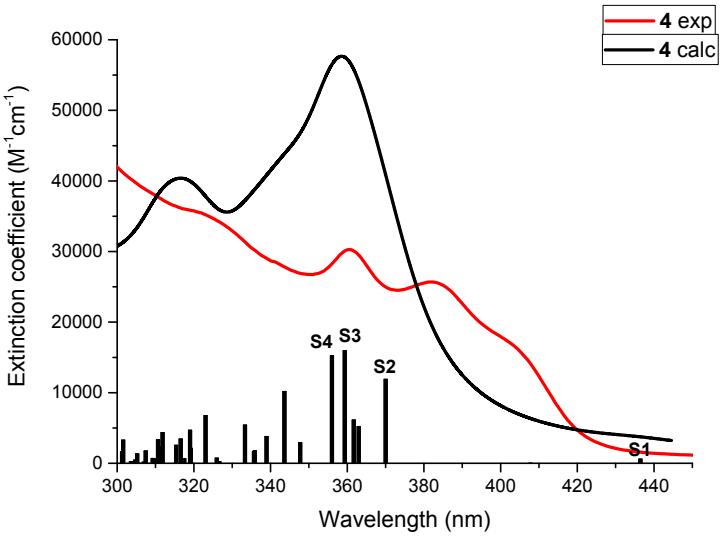

Figure S24. Experimental and calculated absorption spectra of 4. Line halfwidth in the calculated spectrum is 900 cm^{-1}.

Table S13. Experimental and calculated data for absorption spectrum of 4. Wavelength (λ), extinction coefficients (ε), oscillator strengths (f) and NTO contribution in the corresponding transition.

λ, nm (exp)	ε*10^{-3}, M^{-1} cm^{-1} (exp)	Transitions	λ, nm (calc)	*f* (calc)	Contribution of main NTO in transition, %
400sh		$S_0 \rightarrow S_1$	436	0.0078	98
373sh	29	$S_0 \rightarrow S_2$	370	0.1459	80
361	36	$S_0 \rightarrow S_3$	359	0.1954	89
		$S_0 \rightarrow S_4$	356	0.1867	89

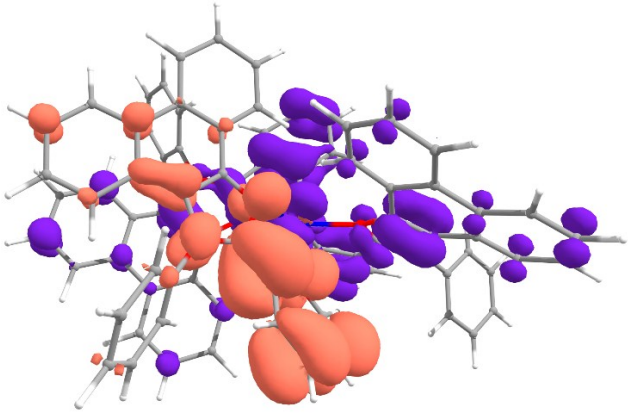

$S_0 \rightarrow S_1$

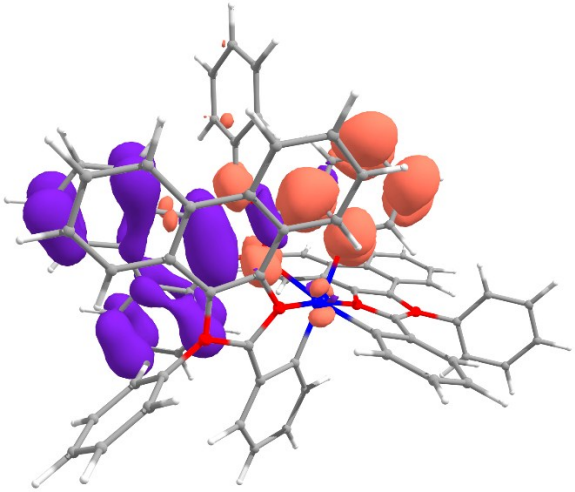

$S_0 \rightarrow S_2$

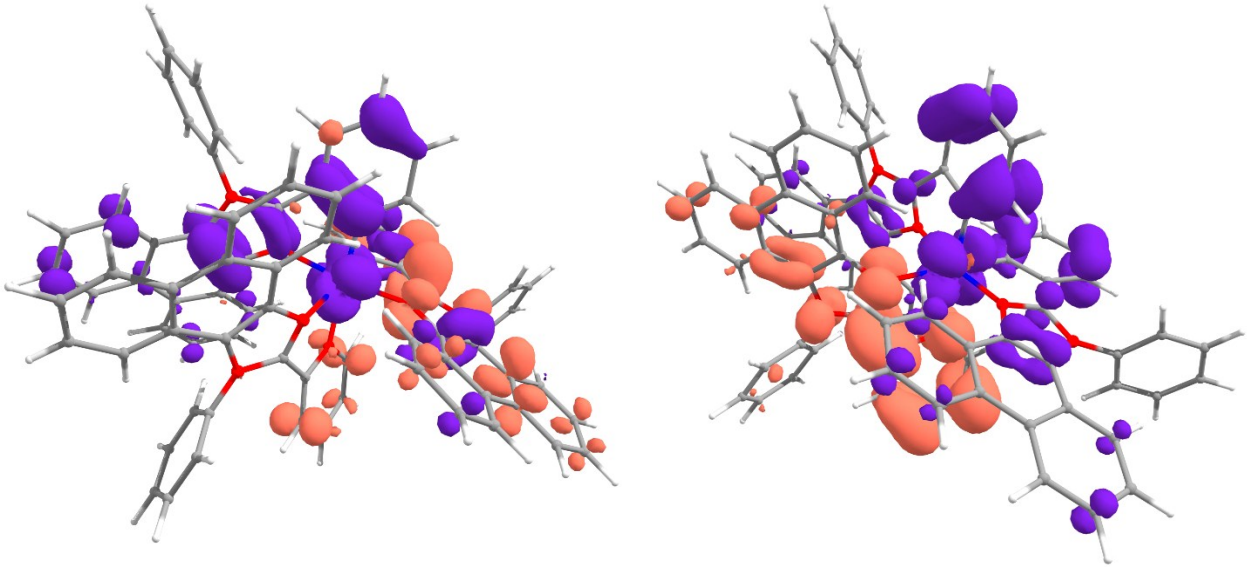

$S_0 \rightarrow S_3$ $S_0 \rightarrow S_4$

Figure S25. Variations in electronic density upon absorption transitions $S_0 \rightarrow S_i$ (i=1-4) of 4. Violet and terracotta denote decrease and increase of electron density, respectively.

Table S14. Interfragment charge transfer (IFCT) for electronic transitions in 4.

S_0-S_1					S_0-S_2				
Donor	Acceptor				Donor	Acceptor			
	Ir	N^N	N^C1	N^C2		Ir	N^N	N^C1	N^C2
Ir	0	0.15	0	0	Ir	0	0.06	0.01	0.01
N^N	0	0.03	0	0	N-N	0.01	0.5	0.01	0.01
N^1C	0.01	0.31	0.01	0.01	N^1C	0	0.11	0.02	0.02
N2^C	0.01	0.43	0.01	0.01	N2^C	0	0.14	0.02	0.03
S_0-S_3					S_0-S_4				
Donor	Acceptor				Donor	Acceptor			
	Ir	N^N	N^C1	N^C2		Ir	N^N	N^C1	N^C2
Ir	0	0.03	0.06	0.06	Ir	0	0.14	0.01	0.01
N^N	0	0.02	0.01	0.01	N^N	0.01	0.26	0.01	0.01
N^C1	0.01	0.05	0.13	0.13	N^C1	0.01	0.21	0.01	0.01
N^C2	0.01	0.07	0.18	0.18	N^C2	0.01	0.22	0.02	0.02

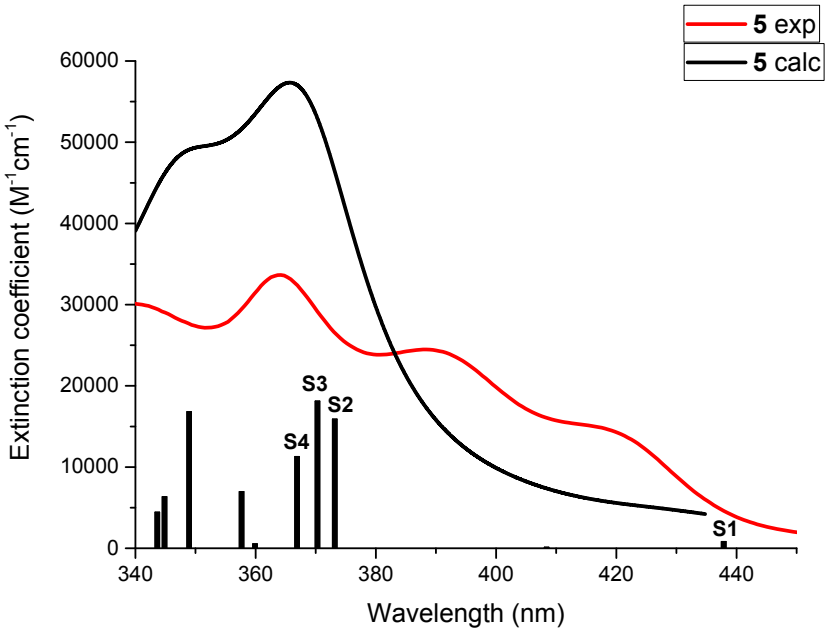

Figure S26. Experimental and calculated absorption spectra of 5. Line halfwidth in the calculated spectrum is 900 cm^{-1}.

Table S15. Experimental and calculated data for absorption spectrum of 5. Wavelength (λ), extinction coefficients (ε), oscillator strengths (f) and NTO contribution in the corresponding transition.

λ, nm (exp)	ε*10^{-3}, M^{-1} cm^{-1} (exp)	Transitions	λ, nm (calc)	*f* (calc)	Contribution of main NTO in transition, %
410sh		$S_0 \rightarrow S_1$	429	0.0107	98
379sh	23	$S_0 \rightarrow S_2$	370	0.1947	52
362	31	$S_0 \rightarrow S_3$	368	0.2218	70
		$S_0 \rightarrow S_4$	364	0.1383	67

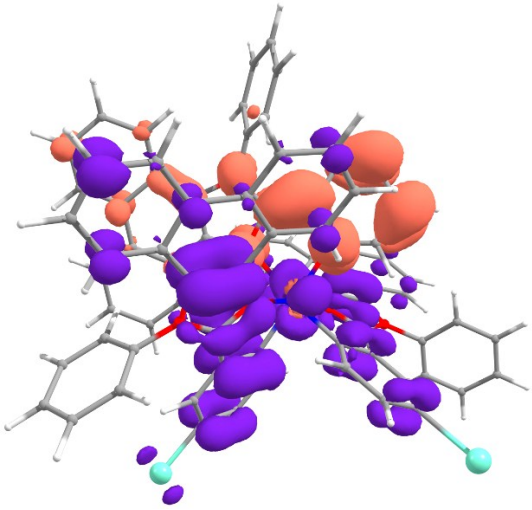

$S_0 \rightarrow S_1$

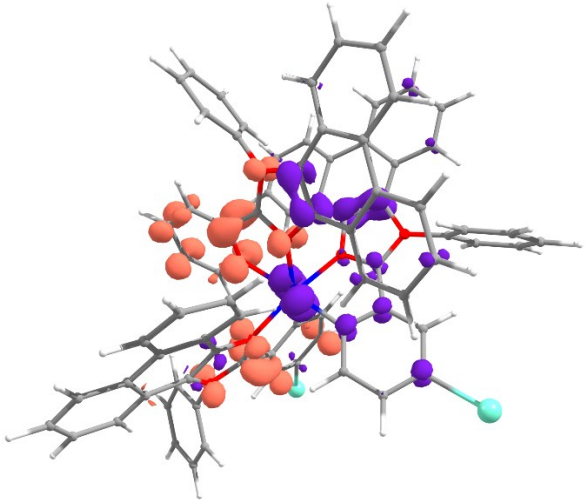

$S_0 \rightarrow S_2$

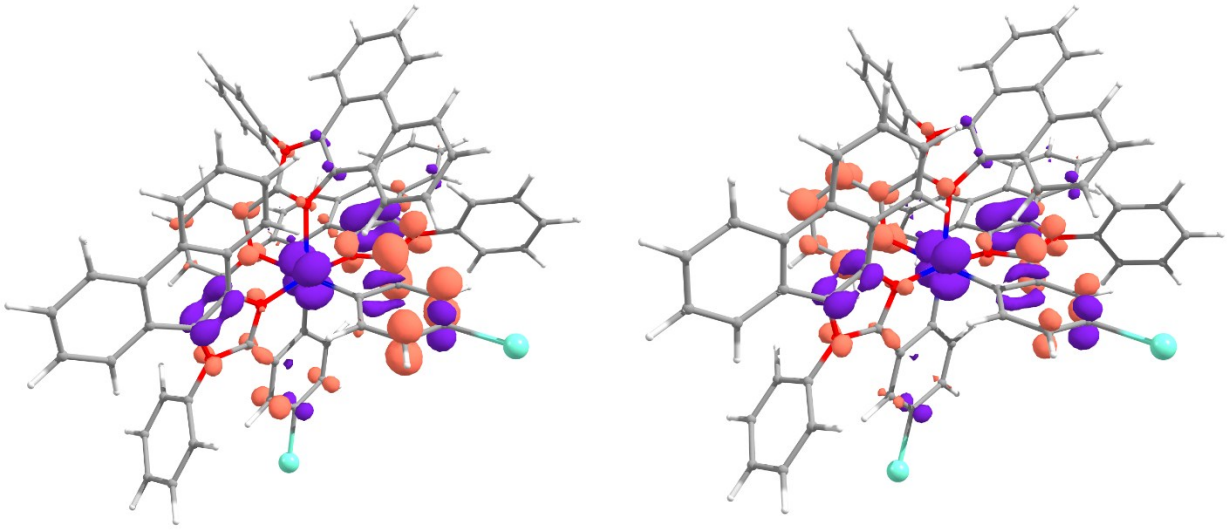

$S_0 \rightarrow S_3$ $S_0 \rightarrow S_4$

Figure S27. Variations in electronic density upon absorption transitions $S_0 \rightarrow S_i$ (i=1-4) of 5. Violet and terracotta denote decrease and increase of electron density, respectively.

Table S16. Interfragment charge transfer (IFCT) for electronic transitions in 5.

S_0-S_1					S_0-S_2				
Donor	Acceptor				Donor	Acceptor			
	Ir	N^N	N^C1	N^C2		Ir	N^N	N^C1	N^C2
Ir	0	0.13	0	0.01	Ir	0	0.02	0.05	0.01
N^N	0	0.04	0	0	N^N	0.01	0.3	0.02	0.02
N^C1	0.01	0.32	0.01	0.02	N^C1	0	0.05	0.13	0.04
N^C2	0.01	0.39	0.01	0.03	N^C2	0.01	0.08	0.16	0.04
S_0-S_3					S_0-S_4				
Donor	Acceptor				Donor	Acceptor			
	Ir	N^N	N^C1	N^C2		Ir	N^N	N^C1	N^C2
Ir	0	0.02	0.04	0.05	Ir	0	0.02	0.04	0.05
N^N	0.01	0.19	0.02	0.03	N^N	0.01	0.2	0.02	0.03
N^C1	0	0.05	0.1	0.12	N^C1	0	0.06	0.09	0.11
N^C2	0.01	0.07	0.12	0.15	N^C2	0.01	0.08	0.11	0.14

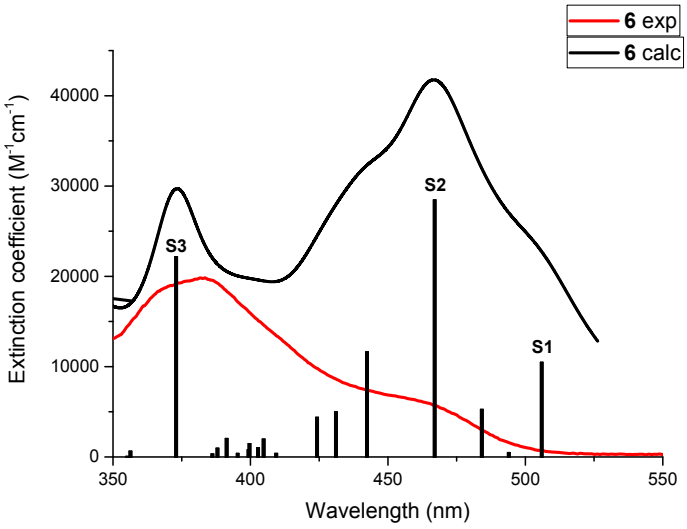

Figure S28. Experimental and calculated absorption spectra of 6. Line halfwidth in the calculated spectrum is 900 cm^{-1}.

Table S17. Experimental and calculated data for absorption spectrum of 6. Wavelength (λ), extinction coefficients (ε), oscillator strengths (f) and NTO contribution in the corresponding transition.

λ, nm (exp)	ε*10^{-3}, M^{-1} cm^{-1} (exp)	Transitions	λ, nm (calc)	*f* (calc)	Contribution of main NTO in transition, %
-	-	$S_0 \rightarrow S_1$	506	0.1286	94
450sh	-	$S_0 \rightarrow S_2$	467	0.348	94
377	-	$S_0 \rightarrow S_3$	373	0.2713	94

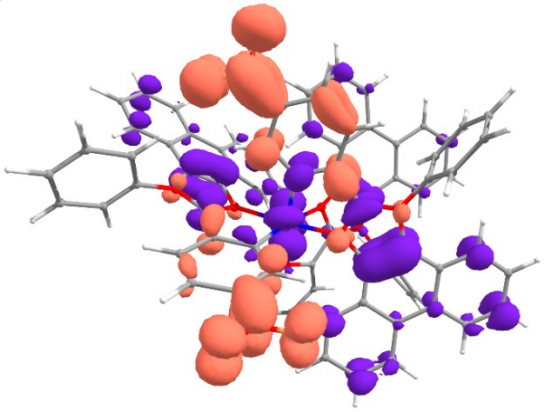

$S_0 \rightarrow S_1$

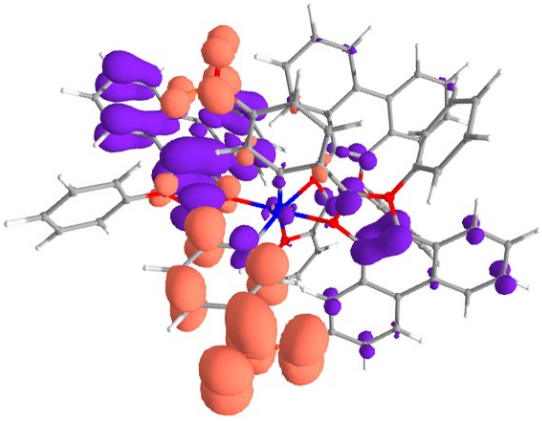

$S_0 \rightarrow S_2$

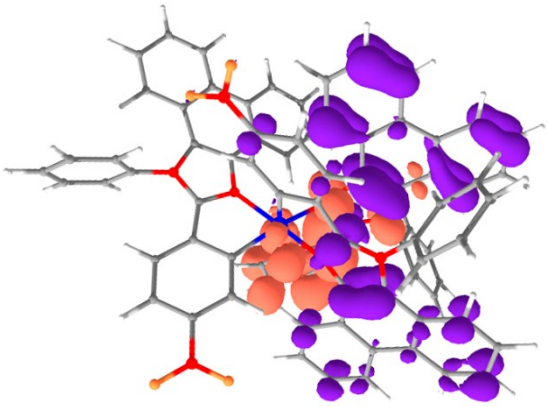

$S_0 \rightarrow S_3$

Figure S29. Variations in electronic density upon absorption transitions $S_0 \rightarrow S_i$ (i=1-3) of 6. Violet and terracotta denote decrease and increase of electron density, respectively.

Table S18. Interfragment charge transfer (IFCT) for electronic transitions in 6.

S_0-S_1					S_0-S_2					S_0-S_3				
Donor	Acceptor													
	Ir	N^N	N^C1	N^C2		Ir	N^N	N^C1	N^C2		Ir	N^N	N^C1	N^C2
Ir	0	0	0.03	0.05	Ir	0	0	0.01	0.01	Ir	0	0	0	0
N^N	0	0	0.06	0.1	N^N	0	0	0.07	0.05	N^N	0.02	0.59	0.01	0.02
N^C1	0	0	0.12	0.18	N^C1	0	0.01	0.36	0.22	N^C1	0	0	0	0
N^C2	0	0	0.15	0.26	N^C2	0	0	0.14	0.09	N^C2	0.01	0.28	0.01	0.01

Table S19. Experimental and calculated ($T_1 \rightarrow S_0$) emission wavelength in dichloroethane. Vibrational structure of the ground state have been taken into account upon calculations.

Compound	λ_{em}(exp), nm	λ_{em}(calc), nm
1	540	502
2	597	557

3	645	610
4	553	510
5	545	559
6	645	619

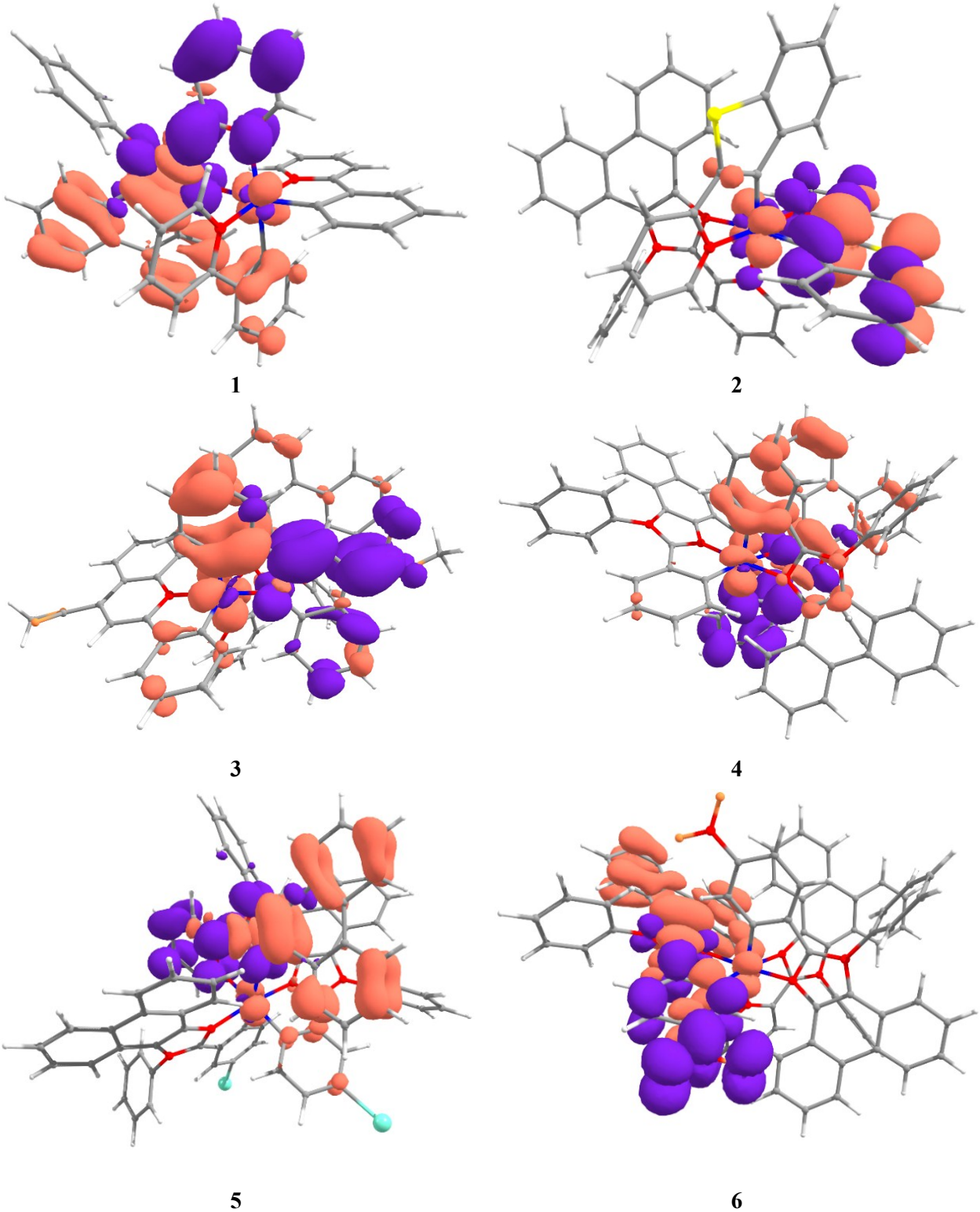

Figure S30. Variations in electronic density upon emissive transitions $T_1 \rightarrow S_0$ for 1-6. Violet and terracotta denote decrease and increase of electron density, respectively.

Table S20. Interfragment charge transfer (IFCT) in 1-6 upon T_1-S_0 transition (in parts of electronic charge).

1					**2**				
Donor	Acceptor				Donor	Acceptor			
	Ir	N^N	N^C1	N^C2		Ir	N^N	N^C1	N^C2
Ir	0.01	0.01	0.01	0	Ir	0.01	0	0.03	0.01
N^N	**0.16**	**0.37**	**0.23**	**0.12**	N^N	0.01	0	0.05	0.02
N^C1	0	0.01	0	0	N^C1	**0.11**	0.03	**0.45**	**0.22**
N^C2	0	0	0	0	N^C2	0	0	0.01	0.01
3					**4**				
Donor	Acceptor				Donor	Acceptor			
	Ir	N^N	N^C1	N^C2		Ir	N^N	N^C1	N^C2
Ir	0.01	0	0.02	0.01	Ir	0	0.01	0	0.01
N^N	0.01	0.01	0.02	0.01	N^N	0.08	**0.29**	**0.14**	**0.36**
N^C1	**0.17**	**0.23**	**0.34**	**0.13**	N^C1	0	0.01	0	0.01
N^C2	0	0	0	0	N^C2	0	0.01	0	0.01

5					**6**					
Donor	Acceptor				Donor	Acceptor				
	Ir	N^N	N^C1	N^C2		Ir	N^N	N^C1	N^C2	Ph-NO_2 (in N^C1)
Ir	0	0.01	0	0	Ir	0	0	0.01	0	0
N^N	0.05	**0.46**	**0.1**	**0.28**	N^N	0	0	0	0	0
N^C1	0	0.01	0	0	N^C1	0.01	0.01	0.1	0.02	0.03
N^C2	0	0.01	0	0	N^C2	0	0	0.01	0	0
					Ph-NO_2 (in N^C1)	0.06	0.04	**0.41**	0.1	**0.14**

Table S21. Comparison of absorption and emission wavelengths of N^C6 and N^C6H$^+$ calculated by various hybrid GGA functionals and experimental ones (DCE solvent).

	N^C6, λ_{abs} (S1), nm	**N^C6H$^+$**, λ_{abs} (S1), nm	**N^C6**, λ_{em}, nm	**N^C6 H$^+$**, λ_{em}, nm
Experiment	**395**	**355**	**620**	**595**
APFD	472	415	601	519
B3LYP	510	–	–	–
CAM-B3LYP	348	–	479	–
HSEH1PBE	494	–	–	–
LC-wHPBE	302	–	–	–
M06	462	–	–	–
M06HF	323	–	–	–
M08HX	351	–	–	–
M11	316	–	–	–
M062X	347	315	469	438
MN12SX	488	430	729	538
MN15	**390**	**351**	**504**	**474**
N12SX	509	–	–	–
PBE0	456	401	561	507

PW6B95D3	448	–	–	–
SOGGA11X	387	–	495	–
TPSSh	559	–	–	–